Identification of Quadrupolar Excitation Channels at the L_3 Edge of Rare-Earth Compounds

F. Bartolomé,[1] J. M. Tonnerre,[1] L. Sève,[1] D. Raoux,[1] J. Chaboy,[2] L. M. García,[2] M. Krisch,[3] and C. C. Kao[4]
[1]*Laboratoire de Cristallographie, CNRS, B.P. 166, 38042 Grenoble, France*
[2]*Instituto de Ciencia de Materiales de Aragón, 50009 Zaragoza, Spain*
[3]*European Synchrotron Radiation Facility, B.P. 220, 38043 Grenoble Cedex, France*
[4]*National Synchrotron Light Source, Brookhaven National Laboratory, Upton, New York 11973*
(Received 7 July 1997)

Resonant inelastic x-ray scattering spectra are recorded at the L_3 absorption edge of rare-earth ions in $R_2Fe_{14}B$. In all cases, weak resonances are observed at energies below the dipolar white line resonance, originating from $2p \rightarrow 4f$ quadrupolar excitations. Their energy position is in excellent agreement with that of preedge features in the x-ray magnetic circular dichroism (XMCD) spectra of the same samples. Our results therefore evidence the systematic appearance of quadrupolar excitation channels and the importance of their inclusion in the correct interpretation of the XMCD at the L_3 edges of rare-earth systems. [S0031-9007(97)04451-7]

PACS numbers: 75.25.+z, 75.50.Bb, 78.70.Dm

The interpretation of x-ray magnetic circular dichroism (XMCD) and x-ray resonant magnetic scattering (XRMS) at the $L_{2,3}$ edges of rare-earth (R) ions, aimed at the determination of important ground state properties such as the atomic orbital and spin magnetic moments via magneto-optical sum rules [1], has been a controversial subject since the first experimental results were obtained [2–5]. It soon became evident that the dichroic signal is not straightforwardly connected to the spin polarization of the R $5d$ band, and the following aspects had to be included: (a) the contribution from quadrupolar excitation channels to the XMCD signal in the preedge region [6]; (b) the effect of the intra-atomic $4f$-$5d$ exchange interaction [7]; and (c) the spin dependence of the radial matrix elements [7,8]. Most of the work so far was focused on aspect (a), and several studies have reported evidence for the quadrupolar origin of some R L_3 preedge dichroic features, using different experimental and theoretical methods: angle- and temperature-dependent XMCD [9,10], XRMS [11–14], resonant inelastic x-ray scattering (RIXS) [15,16], deconvolution of high-quality absorption spectra [17], and atomic multiplet calculations for the quadrupolar part of the absorption spectrum, as well isolated [18,19] as combined with spin-polarized band structure calculations for the dipolar part [20]. More specifically, it has been shown for Gd systems [15,16] that RIXS allows one to separate the dipolar (E1) and quadrupolar (E2) channels by studying the resonance behavior of the $nd^9 4f^{n+1} 5d^0$ and the $nd^9 4f^n 5d^1$ final state multiplets as the incident photon energy is tuned through the $2p^5 4f^{n+1} 5d^0$ and $2p^5 4f^n 5d^1$ intermediate state excitation energies. The two channels can be resolved despite the large $2p$ core-hole lifetime broadening as long as the energy separation between the final state multiplets is larger than the final state lifetime broadening. In contrast, other experimental studies did not show any evidence of E2 character for the XMCD preedge structures in several R ions [3,21–23]. Even more puzzling, an "at-the-edge" dichroic peak lying at the Yb L_3 absorption energy has been interpreted as an E2 signal in $YbFe_2$ [10], while the lower energy feature was assigned to a E1 excitation.

In this Letter we present a RIXS experimental study on the $R_2Fe_{14}B$ series, for which we have already measured the R $L_{2,3}$-edge XMCD [24]. Rare-earth intermetallics are used in the development of high-performance permanent magnets, and the identification of the E1 and E2 contributions to the XMCD is indispensable in order to properly describe the experimental results in terms of rare-earth ($5d$) transition metal ($3d$) band hybridization and $5d$-$4f$ intra-atomic exchange. RIXS spectra are recorded around the R L_3 absorption edge, monitoring the $3d_{5/2} \rightarrow 2p_{3/2}$ radiative decay channel ($L\alpha_1$ fluorescence above threshold) for R = Gd, Tb, Dy, Ho, Tm; or the $4d_{5/2,3/2} \rightarrow 2p_{3/2}$ radiative decay channel ($L\beta_{2,15}$) for R = Nd, Sm, Er [25]. In all cases, at least one additional absorption channel besides the strong E1 $2p \rightarrow 5d$ one is identified, whose excitation energy lies $\approx$5–10 eV below the absorption white line energy. We show a one-to-one correspondence between RIXS and XMCD features below and at the L_3 edge. Although RIXS does not allow a direct multipolar assignment of the observed absorption channels, the E2 origin of the preedge features is convincingly evidenced by its lower energy position and the qualitative agreement with calculations of the E2 part of the RIXS [18,26] and the absorption spectra [19] for the rare-earth series.

The experiments were performed at the beam lines ID16 at the ESRF [27] (for R = Sm, Gd, Tb, Dy, Ho, Er, and Tm) and X21 at the NSLS [28] (for R = Nd). At ID16 (X21) a Si(111) [Si(220)] monochromator provided a 0.5×1.5 (0.5×0.5) mm^2 (horizontal x vertical) beam, linearly polarized in the horizontal plane. The scattered radiation was analyzed in the horizontal plane by a Rowland circle spherical crystal spectrometer with a radius of $\approx$1 m, at 90° scattering angle, thus minimizing the contribution from nonresonant Thomson scattering. The overall experimental resolution was better than 1 eV FWHM

(full width at half maximum) at X21 and in the range of 1–1.5 eV FWHM at ID16. XMCD spectra were measured at the Photon Factory synchrotron radiation facility of the National Laboratory for High Energy Physics (KEK) in Tsukuba. The same powder samples sealed in kapton tape were used in both experiments. A description of its preparation and characterization is given elsewhere [24].

For each sample about 20 spectra were recorded at different fixed incident photon energies $\hbar\omega_1$ around the L_3 absorption edge as a function of scattered photon energy $\hbar\omega_2$ (IXS scans). The whole set of experimental results will be published elsewhere. In Fig. 1 we only show two representative IXS spectra of each studied $R_2Fe_{14}B$ system. The spectra are corrected for self-absorption effects. In order to present the results in a unified picture, the scattered intensity is plotted as a function of a "shifted energy transfer" $E^* = (\hbar\omega_1 - \hbar\omega_2) - (E_{L3} - E_{\mathrm{fluo}})$, where E_{fluo} is the energy of the scattered fluorescence line well above threshold, and E_{L3} the L_3 absorption edge energy. The solid line spectra were recorded at $\hbar\omega_1 = E_{L3}$, corresponding to the largest incident energy at which the maximum of the asymmetric feature, labeled "B" in Fig. 1, remains at $E^* = 0$, indicating that the photoelectron has been excited to a localized intermediate state without acquiring extra kinetic energy. The spectra represented by open circles are taken in the preedge region at an incident energy difference with respect to E_{L3} as indicated in the figure. For the sake of clarity, the spectra have been scaled to the same maximum height, by a factor also displayed in the figure. The spectra recorded at $\hbar\omega_1 = E_{L3}$ are characterized by a single feature with a more or less pronounced shoulder towards $E^* > 0$, while the spectra recorded with $\hbar\omega_1$ in the preedge region show at least one additional feature at energies $E^* < 0$. For heavy rare-earth ions, this feature, labeled "A," is well separated in energy from feature B. For light rare-earth ions, feature A splits into two, labeled A1 and A2 in Fig. 1, appearing as distinct shoulders at $E^* < 0$.

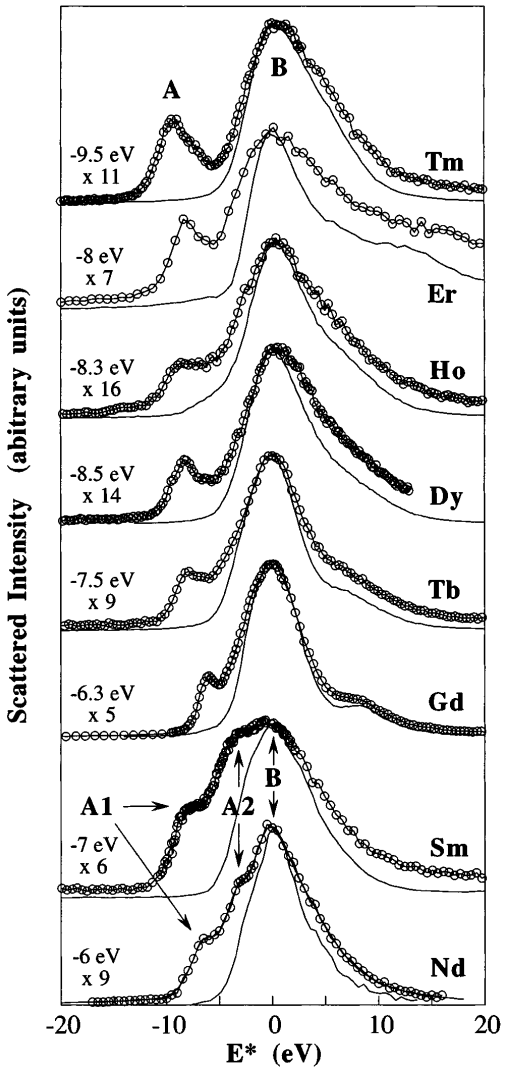

FIG. 1. Resonant IXS intensity (in arbitrary units), recorded at two incident photon energies near the R L_3 edge on $R_2Fe_{14}B$. The scattered energy scale is given by $E^* = (\hbar\omega_1 - \hbar\omega_2) - (E_{L3} - E_{\mathrm{fluo}})$. Full line spectra correspond to $\hbar\omega_1 = E_{L3}$. Open symbols spectra were recorded at $\hbar\omega_1$ lower than E_{L3} by a value displayed in the figure, and are multiplied by the indicated scaling factor.

Previous experimental results [15,16] and theoretical calculations [18,26] allow an unambiguous assignment of features A and B. Features B are assigned to the $nd^9 4f^n 5d^1$ final state multiplets, resonantly enhanced at the $2p^5 4f^n 5d^1$ intermediate state excitation energies, corresponding to the strong dipolar $2p \rightarrow 5d$ channel. Features A are ascribed to the $nd^9 4f^{n+1} 5d^0$ final state multiplets which are resonantly enhanced at the $2p^5 4f^{n+1} 5d^0$ intermediate state excitation energies, corresponding to the weak quadrupolar $2p \rightarrow 4f$ excitation channel. Feature A is observed at lower E^* than feature B, i.e., at smaller intermediate state excitation energies. This is consistent with the strength of the Coulomb interaction between the promoted electron and the nd core hole resulting in a $nd^9 4f^{n+1} 5d^0$ final state more strongly bound than the localized $nd^9 4f^n 5d^1$ or the delocalized $nd^9 4f^n 5d^1 \epsilon^*$ state. Moreover, our assignment is also supported by calculations of the E2 part of the RIXS spectra (for Gd, Ho [26], and Dy [18,26]) and the comparison of the shape of feature A with $3d \rightarrow 4f$ absorption calculations [29] for heavy rare-earth ions, except Er.

In order to directly compare the inelastic scattering spectra with the XMCD spectra, the evolution of the peak intensity of features A (A1 and A2 for Nd and Sm) and B is monitored, scanning the incident and scattered photon energy together, thus keeping the energy transfer $\hbar\omega_1 - \hbar\omega_2$ constant and fixed to values, corresponding to the excitation energies of features A (A1 and A2) and B, respectively [30]. These constant-final-state (CFS) spectra are reported in Fig. 2 (solid lines) together with the corresponding L_3 edge XMCD (open circles) measured on the same samples. It is evident that features A (A1 and A2 for

Nd and Sm) and B correspond to two (three for Nd and Sm) different resonances, attaining their maximum intensity at different incident photon energies. CFS scans corresponding to feature A in heavy rare earths do not show a single peak structure. This fact is partly due to contamination from the tail of the much stronger $nd^9 4f^n 5d^1$ multiplet as the incident photon energy is increased beyond the E2 resonance [31], but also to higher energy E2 excitations, which appear in this range of energies for heavy R ions in calculations of the E2 part of the absorption spectra [18,19].

The correspondence between the resonance energies observed in RIXS and the features in the XMCD spectra below and at the edge is rather evident. In all cases

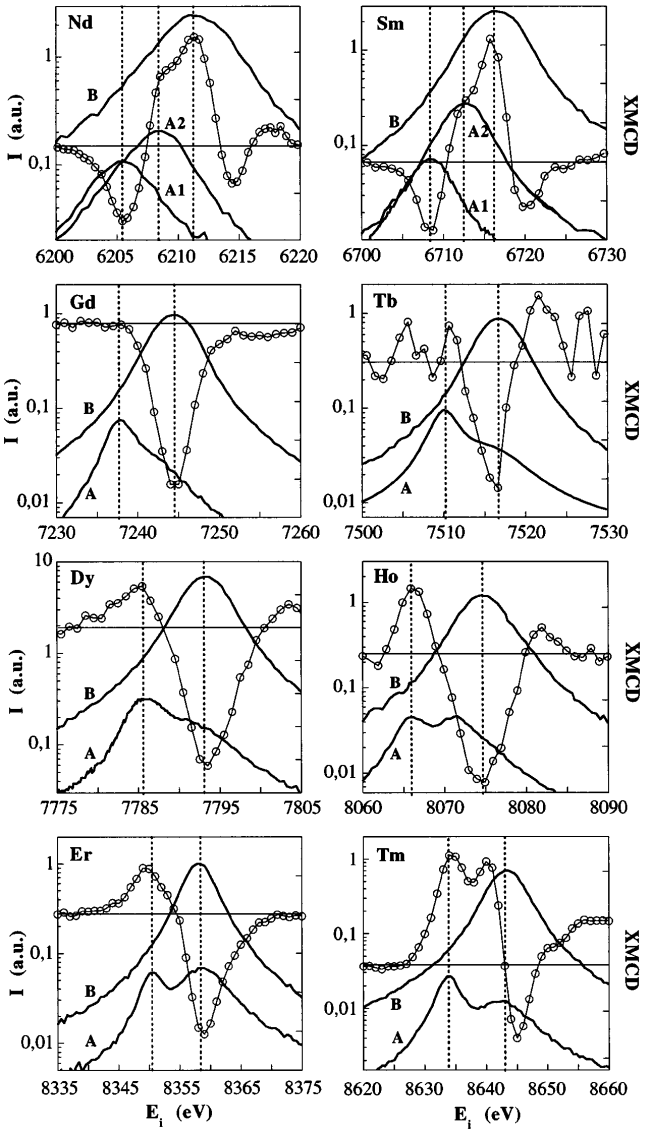

FIG. 2. RIXS constant final state (CFS) scans performed at the energy transfers corresponding to feature A (A1 and A2 for light R) and feature B in Fig. 1 as a function of $\hbar\omega_1$, in comparison with XMCD of the same $R_2Fe_{14}B$ compounds. CFS scans (full lines) are shown in a semilogarithmic scale while XMCD spectra (∘) are shown in a linear arbitrary scale to facilitate a direct comparison. Horizontal lines indicate the zero of the XMCD scale, and vertical dashed lines are guides to the eye.

except Tm, which we discuss later, the energy position around which the E1 resonance is centered corresponds to the strongest feature in the XMCD spectra. This observation is in agreement with the commonly accepted interpretation of the XMCD signal at the absorption threshold. More importantly, most E2 resonances in the CFS scans have their counterpart in the XMCD spectra. The CFS scans of Nd and Sm reveal that features A1 and A2 resonate at two different energies, which coincide with a "negative to positive" double structure in the XMCD. This double structure in Nd and Sm systems can be explained within a simple one-electron picture. We interpret the A1 structure as originated in the promotion of a core electron to a hole in the partially filled "spin-up" $4f$ subshell with the photoelectron spin parallel to the total spin **S** of the $4f$ shell, giving rise to the $2p^5 4f^{(n+1)\uparrow} 5d^0$ intermediate state. Alternatively, the A2 feature corresponds to the E2 excitation to the fully empty "spin-down" $4f$ subshell, with $2p^5 4f^{n\uparrow\downarrow} 5d^0$ intermediate state. The $4f^{n+1}$ configuration related to the A2 feature is more energetic than that to the A1, and has consequently a higher energy transfer in the RIXS spectra. The experimental energy separation between A1 and A2 features is 3.0 ± 0.6 eV and 3.5 ± 1 eV for Nd and Sm systems, respectively, in good agreement with the energy difference between the ground and the first excited terms for $4f^{n+1}$ configurations: 2.5 ± 0.6 eV between ^{5}I and ^{3}K terms of $4f^4$ configuration [32] and 3 ± 1 eV between ^{7}F and ^{5}D of $4f^6$ [33]. As a first approximation, the relative intensity A1/A2 of the two E2 channels should be equal to the ratio of available parallel and antiparallel-spin holes for the photoelectron. For Nd and Sm these ratios are 4/7 and 2/7, respectively. Experimental A1/A2 ratios of $(3.7 \pm 0.2)/7$ for Nd and $(1.9 \pm 0.2)/7$ for Sm are obtained from the integrated signal of CFS scans corresponding to A1 and A2 features. Recent calculations of the E2 $2p \rightarrow 4f$ XAS spectra [19] for Nd and Sm show as well a double peak structure, with an energy separation of ≈2.5 and 3 eV for Nd and Sm, respectively, in agreement with our observation. Moreover, our model explains as well the change of sign of the E2 dichroic signal. Finally, this interpretation is also in agreement with our analysis of XRMS on $Nd_2Fe_{14}B$ [34].

The $Gd_2Fe_{14}B$ XMCD does not show a E2 feature corresponding to the RIXS preedge resonance. However, Gd systems have been studied previously [15,16,26], and the E2 origin of the RIXS resonance is well established. The signal-to-noise ratio in the Tb XMCD prevents the unambiguous assignment of the dichroism at the preedge region to the RIXS E2 resonance. Dy, Ho, and Er are simpler cases; the energy of resonance of the A CFS scan is essentially the same as for the positive preedge feature in the L_3 XMCD spectrum, giving strong evidence of its E2 origin. $Tm_2Fe_{14}B$ presents a three-peaked L_3 XMCD. The energy position of the E2 CFS scan in RIXS coincides with that of the lowest-energy dichroic feature that we ascribe to a E2 transition. The rest of the Tm XMCD has

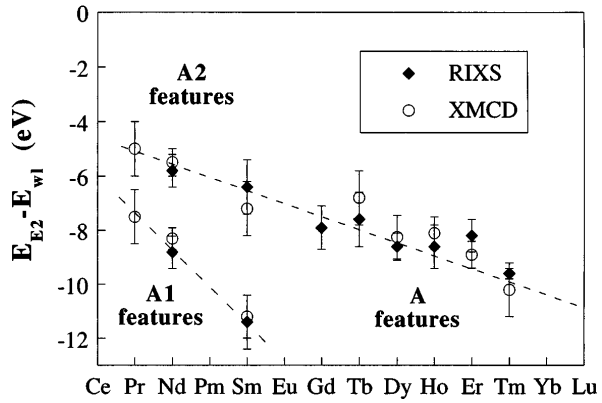

FIG. 3. Energy separation $E_{E2} - E_{\mathrm{wl}}$ between the quadrupolar $2p \rightarrow 4f$ excitation energy, E_{E2}, and the energy corresponding to the maximum of the white line, E_{wl}, as derived from RIXS (◆) and XMCD (∘) as a function of the R element. Dashed lines are guides to the eye.

a dispersive spectral shape, crossing zero between the L_3 edge and the white line energy, E_{wl}. The passage from an absorptivelike to a dispersivelike shape of the E1 XMCD has been recently discussed as an effect of "breathing" of the $5d$ orbitals [7]. It has to be noted that similar spectral shapes have been found in L_3 XMCD signals for Er [23] and Yb [10]. In particular, the Tm XMCD in Fig. 2 is essentially identical to the Yb XMCD recorded at $T = 100$ K on $YbFe_2$, which was interpreted as composed of a E2 contribution at the L_3-edge energy in the middle of a dispersivelike E1 contribution [10]. In contrast, an analogy with our $Tm_2Fe_{14}B$ data indicate that the lowest-energy XMCD peak of $YbFe_2$ would have a E2 origin, with an energy difference with respect to the white line maximum of ~12 eV.

We plot in Fig. 3 the separation in energy between the resonance energy of the E2 features, E_{E2}, and the white line energy, E_{wl}, derived from RIXS (◆) and XMCD (∘) for the $R_2Fe_{14}B$ series. Features A and A2 in heavy and light R, respectively, follow the same trend as a function of filling of the $4f$ shell. This is well understood with the proposed model as the photoelectron is excited to the same $4f$ subshell. The E_{E2}-E_{wl} values as well as its evolution through the rare-earth series are in good agreement with previous theoretical results for $R =$ Gd to Tm [20]. From Fig. 3 we can predict the position of the E2 feature on Yb systems by extrapolating the data to the $4f^{13}$ case, obtaining $E_{E2} - E_{\mathrm{wl}} = 10.5 \pm 1.5$ eV. This value is in very good agreement with a reanalysis of the Yb XMCD in $YbFe_2$ in a similar way as we present it for $Tm_2Fe_{14}B$.

In summary, our RIXS study at the rare-earth L_3 edge in the $R_2Fe_{14}B$ series has allowed us to separately observe the E1 and E2 absorption channels in each rare-earth ion investigated, showing the systematic presence of the E2 channel at energies between 5 and 12 eV below the L_3 white line. The comparison of our RIXS results with corresponding XMCD spectra suggest the E2 origin of the L_3 dichroic preedge features as a general trend in rare-earth systems. A double preedge feature in inelastic and dichroic spectra of light R ions is interpreted as two different quadrupolarly excited final states in terms of a simple one-electron model. This work, together with previous related results [7,9,15,16], should allow in the future the correct interpretation of rare-earth dichroic signals in terms of separate contributions from $4f$ magnetic moments and $5d$ band polarization.

We would like to acknowledge fruitful discussions with F. Sette and F. de Bergevin. This work was partially supported by Spanish DGICYT MAT96-0448 grant.

[1] B. T. Thole *et al.*, Phys. Rev. Lett. **68**, 1943 (1992); P. Carra *et al.*, Phys. Rev. Lett. **70**, 694 (1993).
[2] G. Schütz *et al.*, Z. Phys. B **73**, 67 (1988).
[3] P. Fischer *et al.*, J. Appl. Phys. **69**, 6144 (1991).
[4] F. Baudelet *et al.*, J. Electron Spectrosc. Relat. Phenom. **62**, 153 (1993).
[5] D. Gibbs *et al.*, Phys. Rev. Lett. **61**, 1241 (1988).
[6] P. Carra and M. Altarelli, Phys. Rev. Lett. **64**, 1286 (1990).
[7] M. van Veenendaal, J. B. Goedkoop, and B. T. Thole, Phys. Rev. Lett. **78**, 1162 (1997).
[8] B. N. Harmon and A. J. Freeman, Phys. Rev. B **10**, 1979 (1974).
[9] J. C. Lang *et al.*, Phys. Rev. Lett. **74**, 4935 (1995).
[10] C. Giorgetti *et al.*, Phys. Rev. Lett. **75**, 3186 (1995).
[11] G. Helgesen *et al.*, Phys. Rev. B **50**, 2990 (1994).
[12] C. Detlefs *et al.*, Phys. Rev. B **55**, R680 (1997).
[13] A. Koizumi *et al.*, J. Phys. Soc. Jpn. **61**, 399 (1992).
[14] F. Bartolomé *et al.*, J. Phys. IV (France) **7**, C2-437 (1997).
[15] M. Krisch *et al.*, Phys. Rev. Lett. **74**, 4931 (1995).
[16] M. Krisch *et al.*, Phys. Rev. B **54**, R12 673 (1996).
[17] P. W. Loeffen *et al.*, Phys. Rev. B **54**, 14 877 (1996).
[18] S. Tanaka *et al.*, J. Phys. Soc. Jpn. **63**, 2780 (1994).
[19] M. van Veenendaal and R. Benoist (to be published).
[20] X. Wang *et al.*, Phys. Rev. B **47**, 9087 (1993).
[21] P. Fischer *et al.*, Solid State Commun. **76**, 777 (1990).
[22] P. Fischer *et al.*, Solid State Commun. **82**, 857 (1992).
[23] J. C. Lang *et al.*, Phys. Rev. B **46**, 5298 (1992).
[24] J. Chaboy *et al.*, J. Phys. IV (France) **7**, C2-449 (1997).
[25] The choice of either $L\alpha_1$ or $L\beta_{2,15}$ emission is driven by the availability of a convenient analyzer reflection.
[26] M. van Veenendaal, P. Carra, and T. Thole, Phys. Rev. B **54**, 16 010 (1996).
[27] F. Sette *et al.* (to be published).
[28] C. C. Kao *et al.*, Rev. Sci. Instrum. **66**, 2 (1995).
[29] J. Goedkoop, Ph.D. thesis, University of Nijmegen, 1989.
[30] The energy resolution of the spectrometer was ~0.3–0.5 eV, mainly determined by the horizontal size of the scattering source.
[31] The E1 contamination on the CFS scans at the E2 energy transfer excludes a quantitative determination of the strength of E2 vs E1 excitations, which requires a proper deconvolution of the complete set of IXS scans.
[32] S. Hüfner, Z. Phys. **165**, 396 (1961).
[33] L. G. DeShazer and G. H. Dieke, J. Chem. Phys. **38**, 2190 (1963).
[34] F. Bartolomé *et al.* (to be published).